Chapter 5

Processing Parameters for Selective Laser Sintering or Melting of Oxide Ceramics

Haidong Zhang and Saniya LeBlanc

Additional information is available at the end of the chapter

http://dx.doi.org/10.5772/intechopen.75832

Abstract

In this chapter, we present a detailed introduction to the factors which influence laser powder bed fusion (LPBF) on oxide ceramics. These factors can be in general divided in three main categories: laser-related factors (wavelength, power, scanning speed, hatch distance, scan pattern, beam diameter, etc.), powder- and material-related factors (flowability, size distribution, shape, powder deposition, thickness of deposited layers, etc.), and other factors (pre- or post-processing, inert gas atmosphere, etc.). The process parameters directly affect the amount of energy delivered to the surface of the thin layer and the energy density absorbed by the powders; therefore, decide the physical and mechanical properties of the built parts, such as relative density, porosity, surface roughness, dimensional accuracy, strength, etc. The parameter-property relation is hence reviewed for the most studied oxide ceramic materials, including families from alumina, silica, and some ceramic mixtures. Among those parameters, reducing temperature gradient which decreases the thermal stresses is one of the key factors to improve the ceramic quality. Although realizing crack-free ceramics combined with a smooth surface is still a major challenge, through optimizing the parameters, it is possible for LPBF processed ceramic parts to achieve properties close to those of conventionally produced ceramics.

Keywords: LPBF, SLM, SLS, ceramic, additive manufacturing, AM, processing parameters

1. Introduction

Laser powder bed fusion (LPBF) is an additive manufacturing process that uses a laser beam to fuse powder particles in a layer-by-layer fashion, which allows production of complex three-dimensional (3D) structures. LPBF includes selective laser melting (SLM), where powder is fully melted, and selective laser sintering (SLS) for other cases such as solid state sintering,

liquid state sintering, and partial melting [1]. The main advantages of LPBF are time efficiency and the capability to build geometries that would be unattainable through traditional techniques. LPBF has revolutionized manufacturing by offering great design freedom for 3D structures to be built directly from feedstock powders without additional processing. Introduced in the late 1980–1990s [2–4], the LPBF process was initially applied to metals, and later to polymers, ceramics, and recently, to semiconductors [5, 6].

This chapter focuses on laser powder bed fusion of ceramic materials. Typical ceramics are strongly bonded inorganic and non-metallic solids such as crystalline oxide, nitride and carbide materials. Sometimes non-crystalline or partially crystalline glass is also referred to as glass-ceramic. Ceramics feature excellent strength and hardness, good abrasion resistance, high melting temperature, high chemical stability, low ductility, and low electrical and thermal conductivities.

A classification of processing techniques for ceramic materials is summarized in **Figure 1**. Ceramics cannot be shaped by the conventional forging and machining formation. They are usually formed through multi-step processes [7]. The shaping process begins with powder mixtures that contain binders and stabilizers. The next step is shape forming which includes extrusion, slip casting, pressing, tape casting, and injection molding. The last step is sintering

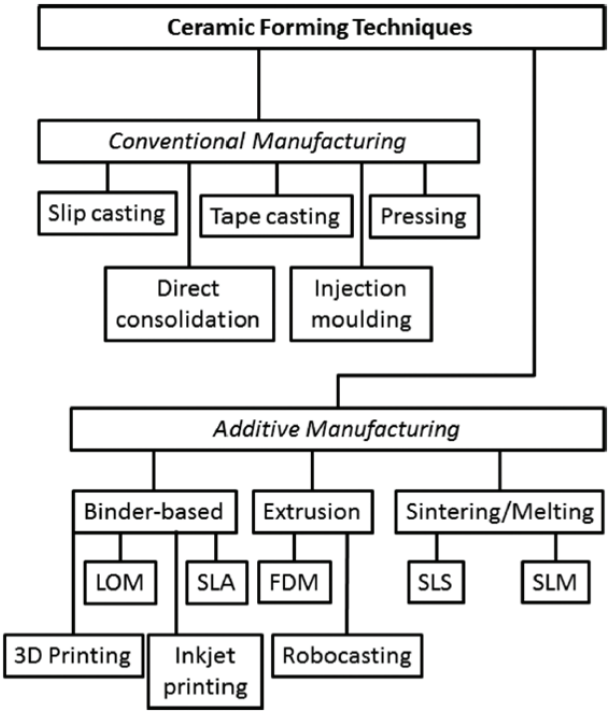

Figure 1. Classification of processing techniques for ceramic materials. Reprinted from [14], with permission of Taylor & Francis Group, LLC.

at high temperatures. These traditional processes involve molding and tooling, have high cost, and limit the device geometry that can be produced.

Additive manufacturing on ceramics has been developed in order to overcome some of subtractive manufacturing's shortcomings, especially with respect to high tool wear, size shrinkage, and difficulty creating complex structures. Additive manufacturing includes binder-based, extrusion-based, and powder-based (LPBF) techniques. Among these, LPBF offers the opportunity for fast and direct fusion without costly post treatments and toxic binders which are often required by other techniques. LPBF-produced ceramic parts have potential to impact several applications such as medical and dental components [8–10], metal casting molds [11], thin wall structures, turbine blades, nozzles [12], and thermal or electrical insulation [13].

While LPBF enables rapid manufacturing of ceramic parts with complex structures, there are two technical limitations. First, ceramic powders, as compared with metals, often flow poorly, resulting in imperfect spreading on the powder bed surface. Second, and more importantly, highly localized heating combined with ceramics' intrinsic low thermal conductivity often leads to large temperature gradients that result in residual stresses and deformation. Combined with ceramics' brittleness, the two limitations can result in cracking, lack of fusion, rough surfaces, porosity and less than full density. Due to these challenges, current results for LPBF of ceramics are far from satisfactory.

There are several excellent reviews for SLS/SLM of ceramics [7, 10, 14–23]. However, many of the SLS/SLM processing factors such as laser power, layer thickness, or powder bed preheating are still poorly investigated or need to undergo a systematic review. Key insights about process parameters have not been transferred into industry. This chapter provides an introduction to LPBF of common ceramics. The chapter is organized as follows. The first part introduces the main procedure and tools for LBPF. Following that, the second section introduces laser parameters, powder parameters, and other factors for the LPBF process, as well as a few physical properties concerned in ceramic applications. The third part discusses how the processing parameters and other factors influence the physical properties of the manufactured parts as well as the general rules for parameter selections. Then the fourth part illustrates some of the most widely studied ceramic materials processed by LPBF, including the state of art achievements. The final two sections summarize the perspectives and the common LPBF challenges for ceramics.

2. Processing parameters and characterization

A basic LPBF system consists of three parts: laser system, powder bed, and spreading system. The laser system includes a laser and a scanner. In order to heat and melt the material, the laser beam has to focus onto the powder surface and be absorbed by the material. The scanner enables the laser to move in a two dimensional plane. The powder bed is a container for the ceramic powders; it usually has adjustable height to allow laser focusing on the newly formed surface. The spreading system often includes a slot feeder to spread fresh powders and a roller or a scraper blade to flatten the surface.

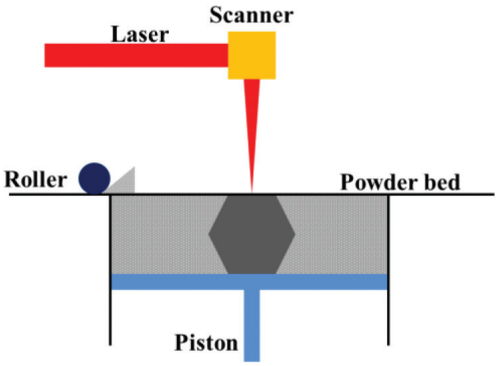

Figure 2. Illustration for basic LPBF procedure.

A typical LPBF setup is illustrated in **Figure 2**. Powders are spread onto the building platform and flattened by a roller, a scraper blade or a combination moving over the surface. The new powder surface moves down one layer thickness to maintain the desired laser focus. The 3D part is decomposed to a number of planes to be processed; each plane consists of a series of basic elements of laser scanning, called vectors. The scan pattern, or the orientation and distance between vectors, is pre-designed. The laser then scans the flat surface of loose or slightly compacted powders following such patterns and selectively melts the illuminated powders. Those powders are quickly solidified after the laser moves away. After that, another layer of powder is deposited and welded, and the process is repeated until a 3D structure in the desired shape and thickness is formed. During the process, unprocessed powder from each layer fills the empty space in the fabrication chamber and supports the part which has been built; afterwards, this powder is recycled. The basic process flow chart is shown in **Figure 3**. Depending on the materials to be processed, the fabrication chamber is sometimes heated and maintained at a certain temperature to help the sintering or melting process. The Renishaw-AM125 (Renishaw, Wotton-under-Edge, Gloucestershire, UK), and SLM@250^{HL} (SLM Solutions GmbH) are two examples of commercial additive manufacturing machines used to process ceramic powders.

LPBF can be broadly classified in two types: direct and indirect, depending on whether a binder material is used. An indirect process either mixes binder materials with ceramics or coats the ceramics with a polymer. The mixture can be used as dry powders or as wet slurry from a suspended liquid. The binder materials melt and consolidate the ceramic powders during laser scanning. Then a de-binding process removes the binder, and further sintering of the ceramic part is usually required to increase the final part density. In the direct process, ceramic objects are created by sintering or melting without the aid of any binders. Because of the high melting temperatures of ceramics, indirect processing of ceramics is most common [24].

2.1. Laser parameters

During the LPBF process, many factors affect the final part. The main laser parameters include wavelength, power, scanning speed, hatch distance, scan pattern, vector length [12], ratio of length to width [25], scan angle [25], beam spatial distribution [26], beam spot size [27], point

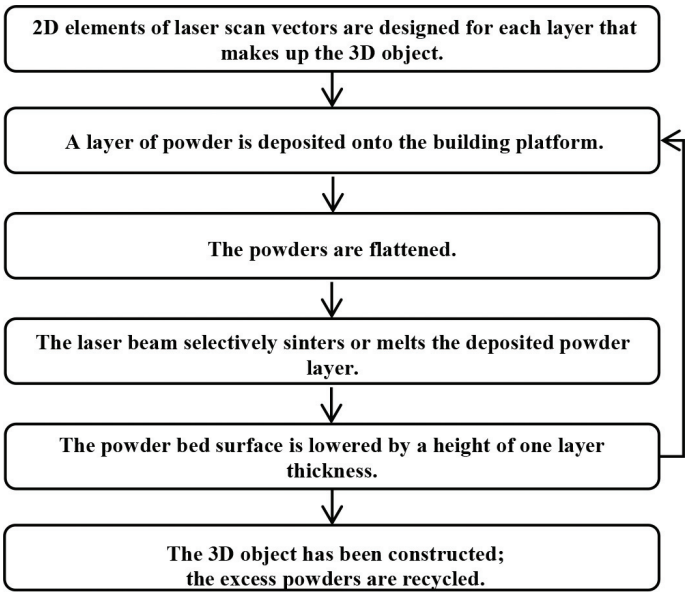

Figure 3. Basic process flow chart for LPBF manufacturing.

overlapping [28], and continuous or pulsed laser operation. Although most of the parameters have an effect on some aspects of the final product, currently there are not enough experimental data or calculations to relate all the factors. Some parameters are not always adjustable, for example, the wavelength of a certain laser system. As a result, only some of the most important parameters will be discussed. Key laser parameters are shown in **Figure 4**.

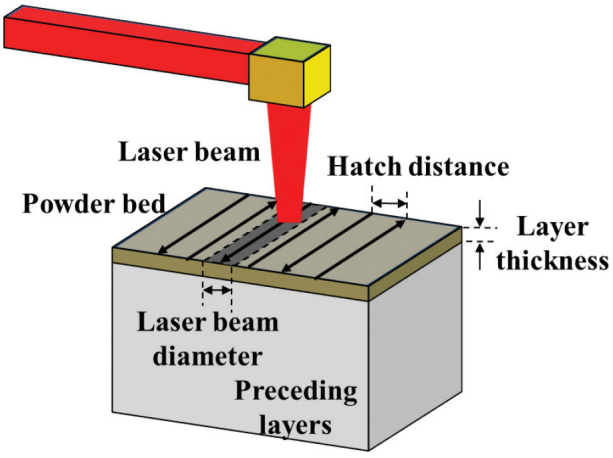

Figure 4. SLM process parameters: laser power, scanning speed, hatch spacing, and layer thickness.

Materials	Absorptance of Nd-YAG laser (λ = 1.06 μm)	Absorptance of CO_2 laser (λ = 10.6 μm)
ZnO	0.02	0.94
Al_2O_3	0.03	0.96
SiO_2	0.04	0.96
BaO	0.04	0.92
SnO	0.05	0.95
CuO	0.11	0.76
SiC	0.78	0.66
Cr_3C_2	0.81	0.7
TiC	0.82	0.46
WC	0.82	0.48

Table 1. Optical absorptance for materials. The data presented here are from those presented in the original source [39].

2.1.1. Laser selection, wavelength (λ), operation mode, and beam diameter (σ)

Laser and powder interactions are fundamental to the LPBF process, and laser selection depends on materials [29–31]. Due to light-matter interactions, materials only absorb light energy for certain wavelengths based on the optical properties. Optical absorption coefficients for some ceramic materials are listed in **Table 1**. Common oxide ceramics only weakly absorb in the near infrared region while carbide ceramics absorb the 1.06 μm wavelength. Therefore, the CO_2 laser ($\lambda \approx$ 10.6 μm) is better suited for oxide ceramics due to higher optical absorptivity, while Nd:YAG, Yb:YAG or Nd:YVO4 ($\lambda \approx$ 1.06 μm) lasers that are common in commercial selective laser melting machines are more suitable to metals and carbide ceramics. Nonetheless, the YAG laser is often applied to oxide ceramics due to its smaller spot size for higher dimensional accuracy, higher specific power, and larger parameter window [28, 32, 33]. The application of the 1.06 μm laser on oxide ceramics is possible because of two effects. First, the absorption for the powder format is usually much higher than the corresponding smooth bulk surfaces due to the multiple reflections effect [34–36]. For example, the optical absorption for alumina is increased to ~10% at ~1 μm [35, 37]. Second, impurities often increase the absorption and reduce the melting temperatures. While it is common to apply a continuous wave laser in the LPBF process, a pulsed laser can also be used [38]. Several additional laser parameters can be adjusted such as pulse durations, shapes and frequencies. It has been shown that those parameters affected the surface quality. Finally, the laser beam diameter or spot size (usually tens of micrometers in diameter) sets the theoretical limit of the spatial resolution although usually many other factors would prevent such a resolution.

*2.1.2. Laser power (*p*), scanning speed (*v*), hatch distance (*h*), and laser energy density (*E*)*

Laser power, scan speed, and hatch distance are the major adjustable parameters are for a laser system. Laser power and the movement of the focused laser spot onto the powder surface should be adjusted to provide enough heat to melt the powers. The hatch distance is the

distance between two neighboring melted lines or vectors; it is usually smaller than the laser spot size. The hatching distance and the spot size decide the overlapping percentage coverage. The three parameters often work together to transfer laser energy to the powder bed. For example, if the absorption coefficient is not very high, it may be compensated for by adjusting one or all of the three parameters. It was reported [40] that a combination of high laser power and low scanning speed helps to reduce balling—the formation of spheroidal beads during the LPBF process due to surface tension and insufficient wetting of the preceding layer [41, 42].

A common practice is to use laser energy density $E = \frac{p}{vh}$ (J/mm^2) [8, 43] or volumetric energy density $\frac{p}{vhd}$ (J/mm^3) [27, 44], or $\frac{p}{v\sigma d}$ (J/mm^3) [45], to represent the laser heating effect, where E is the energy density and d is the layer thickness. Sometimes line energy $\phi = \frac{p}{v}$ (J/mm) has been used instead [46].

2.1.3. Scan pattern and point overlapping

Scan pattern can be single-scan, repeated scan, or cross-scan, with or without contouring. The scan pattern should be chosen based on the material properties and can affect the surface roughness and the mechanical properties of the final product. For example, it was shown that the repeated scan pattern reduced balling [40]. It was reported that contouring helps to generate the same quality for the beginning and ending of scan lines [47]. Also, the contour forms a barrier that keeps the melt pool of the hatch from exceeding the specimen's boundaries [48]. The overlapping of the two parallel, consecutive laser scans is defined as $Ov = 1 - (h/\sigma)$ where h is the hatch distance and σ is the beam spot size [28]. There is an overlap of successive laser spots for $Ov > 0$ and no contact for $Ov < 0$.

2.2. Powder factors

Besides laser factors, powders are also critically affect the LPBF process. Powder size affects laser melting efficiency. Large particles generally reduce the pack density of the powder bed and also require more energy to melt. On the other hand, smaller particles tend to agglomerate, which makes it difficult for powder layering or coating. The typical particle size is in the range of a few to several hundred microns. The ability for powder flow is an important factor to decide the particle distribution on the powder bed. Good powder flow is required to form a flat powder surface and a uniform thickness of powder layers, which are necessary to achieve uniform laser energy absorption. Particle morphology and size distribution affect the powder flow, for example, in general powders flow better with the increase of the sphericity and particle size for particles with a narrow size distribution [9, 12, 49]. The "flowability" in turn significantly affects packing efficiency, mechanical properties, and surface roughness. Powder composition, melting point, optical properties, and heat transfer properties also affect the choice of laser parameters and final product properties. Although these powder factors are important, systematic studies on them are lacking. The powder layer thickness is a very important factor, and it needs to be determined according to the laser beam penetration to the powder bed. Layer thickness also affects the energy density to be applied and can affect the surface roughness [50].

2.3. Other factors

Other factors also significantly affect the LPBF process, including pre- or post-processing, secondary laser assistant, application of protective gas atmosphere, etc. The preheating decides the temperature of the powder bed and is particularly important in the case where binders are used since it affects the wetting and spreading properties. Oxidation usually happens if the process is not in an oxygen-deficit environment, which affects the materials' structure and properties.

The laser beam characteristics and scanning fashion, together with the optical and thermal properties of the powder layer, govern the balance between heating by the absorption of laser radiation and conductive thermal losses. The thermal absorption and dissipation dictate the temperature of the laser-powder interaction zone [51]. With appropriate combinations of laser parameters and proper powders, the interlayer bonding strength and the mechanical strength of the whole component can be improved [52].

2.4. Quality assessment

Depending on the purpose of applications, attributes of the final products are assessed to determine part quality. Critical attributes are porosity, relative density, surface roughness, dimensional accuracy, strength, micro hardness, and other mechanical properties.

Pores often form in the LPBF processed products. Porosity, the percentage of void space in a bulk material, is hence an important parameter for the laser treated materials. The porosity content can be determined by an image analysis method [53]. Relative density is the ratio of the LPBF-processed part density to the theoretical density of the bulk material. Relative density is a basic parameter of the product. Because of the direct relation between relative density and porosity, it is common to measure relative density instead of porosity since relative density is easier to measure.

Surface roughness measures the surface irregularities, often expressed as numeric parameters R_a and R_z, where R_a is the arithmetic mean deviation of the roughness profile, and R_z is the maximum roughness, or the maximum height of the profile from peak to valley. LPBF of ceramics often leads to a poor surface finish and high roughness because the melt pool is large, and the molten material has low viscosity and thermal conductivity. It was shown that low viscosity large melt pool wet the powders outside the pool boundary, and led to large grains and rough surfaces [48, 54, 55].

Dimensional accuracy is the measure for the accuracy of the LPBF product to the expected parts. The material's strength is the measure to withstand an applied maximum stress without failure, including compressive, tensile, and shear strengths. Because of cracks and pores, LPBF ceramics have lower strength than their cast counterparts. An important indicator for the mechanical properties for the LPBF product is the bending strength. A positive linear relationship between bending strength and relative density has been reported [56], so relative density can be an indicator for bending strength. Hardness measures the material's ability to resist permanent plastic deformation.

Using LPBF as the manufacturing technique, the important difference between ceramics and metals is that ceramic materials are particularly subject to cracks and delamination [21] due to the large thermal gradient resulting from ceramics' intrinsic very low thermal conductivities and very high melting temperatures. Compared to metals, the LPBF-produced ceramics often display lower relative density and rougher surface. While steels made by SLM process are often mechanically stronger than those made by casting [21], currently SLM-manufactured ceramics are almost always mechanically weaker than their counterparts made from conventional methods. Therefore, applying LPBF to ceramics generally presents more challenges than that to metals.

3. Principles for optimum SLM/SLS process

Both direct and indirect methods are capable of processing ceramics close to a full density. The advantage of the direct process method is that post-processing is not required for the parts manufactured, and it is possible to directly manufacture near crack-free ceramic parts with high densities [9]. However, because of the very high melting point, it is common to coat the pure ceramic powder with binders, to make use of the existing or mixed absorption impurities, or to form some sort of low-melting point eutectics with several ceramics. In those cases, a post-processing thermal treatment is often necessary to obtain denser parts.

Both a CO_2 laser and a YAG laser can be used for processing ceramics. On the one hand, the longer wavelength CO_2 laser corresponds to higher optical absorptivity. On the other hand, the YAG laser yields better dimensional accuracy due to its much smaller laser spot size. However, in order to use the near-infrared laser, additive materials are often mixed with the ceramics to improve laser absorption. The additives are chosen to strongly absorb the laser beam but not to react with ceramics at high temperatures. Many materials can be used for such a purpose. For example, they can be low-melting-point polymers that are eventually burnt off or inorganic powders such as graphite, and sometimes the existing impurities can work as the absorption medium to increase the laser-material coupling.

A suitable setting of laser processing parameters can improve microstructures and the mechanical quality of the processed parts. However, optimizing one single parameter or process usually accompanies other disadvantages for the ceramic process. The choice of a process for a particular design requirement often involves a compromise of other properties. No universally good parameters or processes exist for ceramics processing at this time. Even for the same material, the most common adjustable parameters, such as laser power, scanning speed, hatch distance, and laser spot size, can vary wildly depending on the requirement of a better mechanical strength or a better surface finish. The parameters are crucially dependent on the existence and variety of additives. For example, very different parameter sets for processing alumina exist (**Table 2**) [27, 28, 55, 56]. Additionally, the parameters also relied on powder and layer factors as well as preheating conditions. On the other hand, for each individual experiment, there are clear trends regarding the laser parameters. Some of the basic trends are summarized below.

	Powder size (μm)	Layer thickness (μm)	Laser wavelength (μm)	Laser beam diameter (μm)	Laser power (W)	Scanning speed (mm/s)	Hatch distance (μm)	Energy density (J/mm^2)	Relative density (%)	Other conditions
Al_2O_3 coated by PVA + resin E06 [56]	80	—	—	—	15, 18, 21	1600, 1800, 2000	100, 120, 140	0.088	94.6	Postheat @ 1600°C
Al_2O_3 + 0.1 vol% graphite, slurry [28]	106	50–100	1.064	69	100–150	—	50–400	5.1–19.9	97.5	—
Al_2O_3 slurry [55]	0.3	50–200	10.6	400	2	5.2	200	1.9	85	Preheat @ 800°C; postheat @ 1600°C
Al_2O_3 suspension [27]	0.45	—	10.6	1.5–2.5	72	4	—	9	—	Preheat @ 2000°C

Table 2. Parameters for LPBF process on Al_2O_3.

Laser energy density is a very important factor in the LPBF process. In general, the adjustment of parameters that increase the laser energy density results in greater fusion ability as demonstrated by a deeper laser penetration depth or a larger melting pool. Increase of the energy density may be realized through increasing the laser power, decreasing the scanning speed, increasing the hatch distance, using a better focus of the laser beam or changing the laser beam size, or increasing the point overlapping. On the one hand, it was difficult to construct ceramic parts successfully due to insufficient solidification of powders with too low laser energy. On the other hand, high laser energy density induces layer shrinkage because of powder layer overheat or ablation, and the ceramic part warps [57]. Energy density crucially affects the relative density and porosity of the laser processed part [27], but the laser energy density and the relative density of the product do not always follow a positive relation. Wang et al. reported that at the region of low laser energy density, the relative density of the produced part increased with the laser energy density, but after a certain value, a further increase of the laser energy density reduced the relative density of the part [56]. Energy density also severely influences the surface conditions and grain sizes of the laser produced parts. Shishkovsky et al. reported larger mosaics on the surface by reducing the energy density through increasing the laser scan velocity and the hatch distance [13]. Yap et al. reported sunken cores for the samples obtained at higher energy densities, suggesting that vaporization of silica material occurred during the process as the silica material absorbed enough energy to be vaporized [58].

Although the concept of energy density is very useful, practically it has to be adopted with caution because there is sufficient evidence to show inconsistent or controversial results if process optimization is only based on this factor. Wang et al. showed a huge difference in the relative density by similar laser energy density while varying the laser point overlapping [56]. Liu et al. also reported the same energy density led to different relative densities and mechanical properties [59]. The issue of the laser energy density has also been noted by the latest research. Because the laser energy density is insufficient to capture the complex physics of the melt pool, this parameter is identified as an unreliable indicator or not a good design parameter for materials' synthesis by LPBF methods [38, 60]. Although the energy density remains constant, the variable combination of the laser power, the laser scanning speed, and the laser hatch distance plays a significant role, and the laser power has a dictating influence [38]. Liu et al. noted that the influence for the three adjustable laser parameters are not the same to the manufactured parts, precisely, the laser power has the greatest effect, the laser hatch distance is in the middle, and the laser scanning speed has the least effect [59]. However, the different effects among those parameters are not reflected in the concept of the laser energy density. Therefore, the laser energy density cannot be the only criterion in the optimization of process parameters during the SLS/SLM process. An optimum process has also to involve additional process parameters, such as hatch style, laser spot size and laser offsets, and materials properties, including thermal conductivity and reflectivity [38].

Besides laser parameters, powder factors also play a critical role in reaching a high density part. The size and morphology of the powder particles have strong impacts on the powder bed density and the powder flowability and hence significantly influence the product. In order to uniformly spread powders to a thickness of tens to a few hundred microns at high temperatures, a good flowability is critical, which requires powders of specific size distributions and

spherical shape. In general, small particles lead to a better surface, and the spherical shape of particles leads to better flowability and less porosity. Hagedorn et al. reported the surface roughness may be improved by decreasing the particle size from 50 to 30 μm [48]. Wilkes et al. demonstrated that spherically shaped particles significantly improved the relative density and porosity [9]. The method of preparing the powder bed and the layering step are important factors, and optimal processes may lead to sizable improvement of the product. The powder bed should be homogeneous, have high packing density and have a stable layer thickness. Bertrand et al. suggested increasing the powder bed density by compression from the roller [12]. Juste et al. also suggested increasing the powder bed density to decrease the cracks and heterogeneities through the use of more suitable powders and/or by considering specific devices to pre-compact the powder bed [28]. Wang et al. compared the experimental and simulated relative density under different pressures and revealed a positive relation between them, as shown in **Figure 5** [56]. Compressing the powder bed or each powder layer to a denser format before or during each laser scan cycle should be considered for future development in the LPBF process.

The layering step and the deposition technique are critical parts of direct-layered fabrication technologies. For example, Deckers et al. deposited layers through the electrophoretic deposition (EPD) method to avoid large particle and thermal gradients [55]. They suggested slurry-based processes can produce highly dense ceramic parts more easily. Juste et al. also showed good relative density parts using the slurry process [28]. However, this wet process required additional steps. Finally, in the layer-by-layer method, the thickness of each layer is recommended to satisfy the following requirement for a good fusion. Several researchers noted that particles to be ten times smaller than the layer thickness [12, 61], and Bertrand

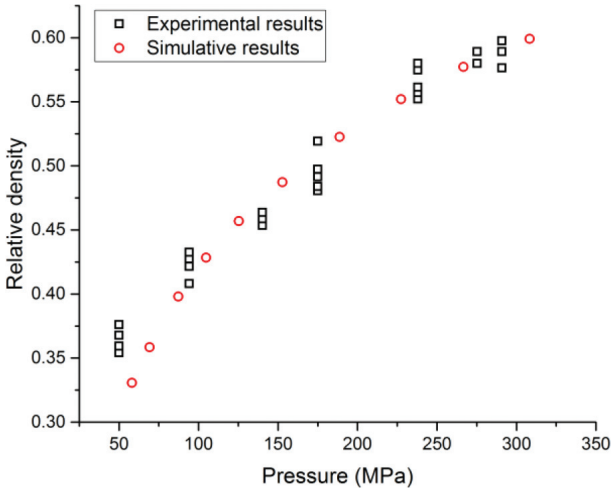

Figure 5. Comparison between the experimental and simulated results of the relative density under different pressures. The data presented here are extracted from those presented in the original source [56].

et al. suggested that each layer allow the laser to penetrate at least through the last and the previous one [12]. A proper combination of laser and powder parameters may lead to the desired properties; for example, the laser power, the layer thickness, and the scanning speed greatly affect shrinkage, distortion and warping, which in turn affect the quality and dimensional accuracy of the parts [62].

Cracks and less than full density are common difficulties in laser processed ceramics. Preheating of the powder bed helps form a denser part and to reduce cracks that are created due to stress and lack of thermal relaxation. Hagedorn et al. reported reaching nearly 100% relative density using a secondary laser as the preheating source [48, 54]. However, this method suffers from bad surface quality for the produced part. Wilkes et al. reported generally crack-free samples through a preheating process showing that powder bed preheating reduces thermal stresses and the formation of cracks [9], but superficial microcracks still existed for large parts during the process [48, 54, 63]. The fine cracks are presumably formed due to thermal stress from the uneven distribution of heat within the laser spot, which induces different volume contractions during the melting and cooling process [64]. Although preheating and secondary laser assistance may reduce the thermal stress and help to reduce cracks, the preheating may decrease the powder flowability and impair the process repeatability [12]. A new preheating strategy to avoid the rapid cooling and the thermal stress requires further technological developments.

Another factor affecting the process is the oxygen environment, and the impact of this factor is strongly material dependent. A low oxygen environment significantly reduces the occurrence of balling [40, 41, 65]. Shishkovsky et al. compared the alumina–zirconium ceramics synthesis in both air and argon environments and found an oxygen-deficit environment clearly affected the light energy absorption, the porosity, and the mechanical strength [13]. Savchenko et al. recommended sintering zirconium in an inert gas environment or in a vacuum for stabilization of the tetragonal phase ZrO_2 [66].

Today normal SLS/SLM techniques are capable of achieving near full relative density for ceramics, but the resulting ceramics are often compromised by high surface roughness, poor dimensional accuracy, micro-crack formation problems, and poor mechanical properties. In recent years, new developments in LPBF have shown some improvement in these aspects. Exner et al. demonstrated a laser micro sintering technique using a q-switched pulse laser system with 532 nm wavelength to process silica-alumina (SiO_2/Al_2O_3) powder [67]. The intensity of the laser spot of the q-switched beam is a factor of several orders of magnitude higher than that of continuous wave lasers due to its short intense pulses in a nanosecond regime, and a very high recoil pressure was generated for the sintering process. In order to obtain good accuracy and surface finish, fine powders with particle diameter less than 1 μm were used. The final parts had a high geometric resolution of 40 μm, the best surface quality so far, with an average surface roughness $R_a \sim 5$ μm, and a maximum relative density of 98%. The produced part still had many small pores and micro cracks inside the sintered body. After thermal treatment, the cracks were annealed, and the number of pores decreased although some bigger pores were left. The heat treatment resulted in nearly no shrinkage (<0.7%) of the specimens. The paper also reported a maximum crushing strength of 1400 MPa, and a low tensile strength of 120 MPa that limited its use in high strength components.

4. Exemplars

With the principles being discussed, it is useful to look at actual examples for some of the most common ceramics: alumina, silica, and mixture of oxide ceramics. These examples are selected to cover ceramic fusion through both direct and indirect methods, SLM and SLS, short (1.06 μm) and long (10.6 μm) laser wavelengths. They also show comparisons for various conditions such as different sized powders, different laser energy densities, with and without preheating or postheating, in air and oxygen-deficit environment, etc. However, the following exemplars do not constitute a completed survey; rather, representative examples are selected to show some of the best progress in the field so far. Some of the processing parameters are summarized in **Tables 2–4** which are slightly different as not all parameters were reported or available in most papers.

4.1. Exemplar I: Alumina (Al_2O_3)

Aluminum oxide, also known as alumina, is often used as an abrasive or a refractory material due to its high hardness, temperature and electrical resistance. Pure Al_2O_3 melts at 2072°C. Some research on this material takes the indirect route due to the high melting point, but direct SLS/SLM is also possible although it often requires very fine (sub-micron) powders.

The following discussion illustrates the indirect method, the effect of post-heating, and the choice of laser energy density. Wang et al. reported using the indirect method to process alumina [56]. The sample was α-Al_2O_3 coated by 1.5 wt.% polyvinyl alcohol (PVA) and then mixed with epoxy resin E06, forming spherical powders with a size of 80 μm. The processing parameters were: laser power between 15 and 21 W, a scanning speed between 1600 and 2000 mm/s, and a scan space between 100 and 140 mm. The paper reported the optimized energy density of 0.088 J/mm^2, which resulted in a relative density of 34% with a bending strength of 1.05 MPa. Post-processing sintering was necessary for densification. Post-process sintering helped to increase the migration rate, grain growth and pore exclusion. After 4 h at 1600°C, the relative density reached 94.6%, a 178% improvement. The relative density increased with increasing laser power and decreased with increasing hatch distance.[1] The relation of the relative density to the scanning speed was more complex in that it initially decreased and then increased with increasing scan speed. Considering the three separate processing parameters, there was an optimum laser energy density which achieved the largest relative density, as shown in **Figure 6**.

The following example shows the SLM process, the effect related to laser point overlapping and layer thickness. Juste et al. mixed alumina powders with 0.1 vol.% graphite to increase the absorption of the Nd:YVO_4 laser (1.064 μm) [28]. Graphite was used as the absorption additive because experiments for the pure alumina were not successful, even with a laser power up to 200 W. The slurry of alumina and graphite-based colloidal suspension mixture was spray-dried and then processed in an Ar environment. By optimizing the parameters, a relative

[1] 'Scanning space' as used by the original source [56] is interpreted as hatch distance here.

	Powder size (μm)	Layer thickness (μm)	Laser wavelength (μm)	Laser beam diameter (μm)	Laser power (W)	Scanning speed (mm/s)	Hatch distance (μm)	Energy density (J/mm^2)	Surface roughness (μm)	Compress strength (MPa)	Dimensional accuracy (mm)	Porosity (%)	Other conditions
SiO_2 [58]	—	100	1.06	80	100	100	40–60	16.7–25	—	—	—	—	—
SiO_2 (slurry of 60 wt.% power + 40 wt.% sol) [57]	10–16	100	10.6	—	6.5	120	100	0.54	—	—	—	—	—
Silica sand [11]	—	200	10.6	300	160	120	200	6.7	~36	—	0.4	—	Post process: infiltration
Silica sand (SiO_2 + a little Al_2O_3) [68]	50	150	10.6	—	120	120	200	5	24.8–28.2	11.8–13	—	—	Preheat @ 400°C
2% PF + silica sand [46]	98	300	1.06	50	5–8	300–500	—	10–20 J/m (line energy)	—	0.8	—	25.7–36.9	—
8.3% PF + silica sand [52]	—	—	10.6	3000	12	10.8	2500	0.44	—	—	—	—	—

Table 3. Parameters for LPBF process on SiO_2

http://dx.doi.org/10.5772/intechopen.75832

	Powder size (μm)	Layer thickness (μm)	Laser wavelength (μm)	Laser beam diameter (μm)	Laser power (W)	Scanning speed (mm/s)	Hatch distance (μm)	Energy density (J/mm^2)	Relative density (%)	Bending Strength σ_{fM} (MPa)	Surface roughness (μm)	Dimensional accuracy (μm)	Other conditions
SiO_2-P_2O_5-CaO [8]	5–10	50–150	10.6	300	5–25	50–300	—	1.5	72	4.7	25	—	Post-heat @ 1200°C
K_2O-Al_2O_3-SiO_2 [59]	5–25	80	10.6	200	21	1800	100	0.1167	36.45	2.08	—	—	Preheat@ 30–35°C
ZrO_2-Y_2O_3 [12]	1–40	30	1.064	—	—	1250–2000	20–40	—	56	—	—	—	—
YSZ-Al_2O_3 [48, 54]	—	50	1.06	200	60	200	—	—	~100	500	100	150	2nd laser, preheat@ 1600–1730°C
YSZ-Al_2O_3 [9]	20–70	50	1.06	200	60	200	—	—	~100	538.1	—	—	2nd laser, preheat@ 1570–1800°C
YSZ + Al/Al_2O_3 [13]	—	—	1.06	80	50	1500–2000	20–40	0.625–1.67	—	—	—	—	In air/Ar environment; laser defocalization ~ 6 μm

Table 4. Parameters for LPBF process on ceramic mixtures.

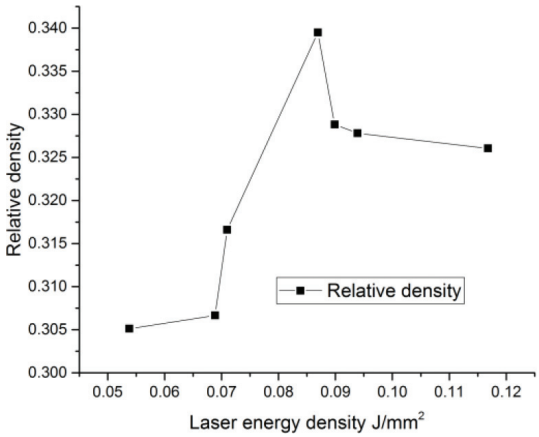

Figure 6. The laser processed Al_2O_3-resin E06 composite reached the peak relative density value of 0.34 when the laser energy density was approximately 0.088 J/mm^2. The data presented here are extracted from those presented in the original source [56].

Figure 7. Pure alumina parts processed by SLM. Reprinted from [28], with permission of Cambridge University Press.

density greater than 90% was achieved. An example of the SLM processed parts is shown in **Figure 7**. The correlation between the product's relative density to the laser energy density and point overlapping is shown in **Table 5** and **Figure 8**. Energy density directly affects the relative density; however, it cannot be used as the single laser parameter for SLM/SLS processes. For example, laser point overlapping had a significant influence on the geometrical features and microstructures of the product [69]. Juste et al. [28] further explored the effects of layer thickness and found a relative density increase from 76.9 to 85.1% by decreasing the layer thickness from 100 to 50 μm. The SEM micrograph showed a microstructure with smaller pore size, suggesting a better welding between two consecutive layers from a more homogeneous and efficient melting. Hence, a decrease in layer thickness improved the microstructures and the relative density of parts.

Experiment	Relative density (%)	Energy density, j (J/mm^2)	Point overlapping, Ov (%)
E2	57.2	5.1	−44
E5	67.3	6.3	−44
E8	76.9	7.6	−44
E3	0.0	5.3	−477
E6	0.0	6.6	−477
E9	0.0	7.9	−477
E1	92.9	13.3	28
E4	97.5	16.6	28
E7	97.3	19.9	28

Table 5. Relative densities vs. laser energy density and point overlapping. The data presented here are from those presented in the original source [28].

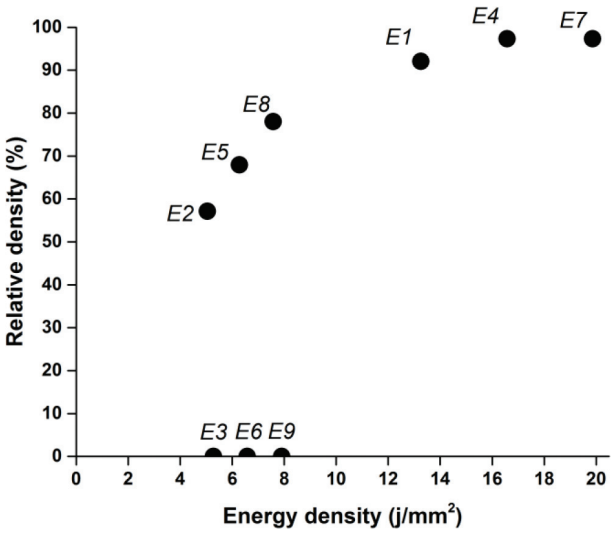

Figure 8. Relative density of laser produced part vs. laser energy density The data presented here are extracted from those presented in the original source [28].

The following two examples demonstrate the direct method without any binders, and they also show how layer deposition is critical for LPBF technique and the effect of varying laser energy density. Deckers et al. used a CO_2 laser for direct SLS/SLM on alumina slurry mixed with very fine (0.3 μm) powders of alumina, denatured ethanol, and HNO_3 [55]. The layers were then deposited through electrophoretic deposition (EPD). The combination of small powders, EPD deposition, and high preheating temperatures (800°C) reduced the need for large energy density to process the alumina slurry without binders. This treatment helped to

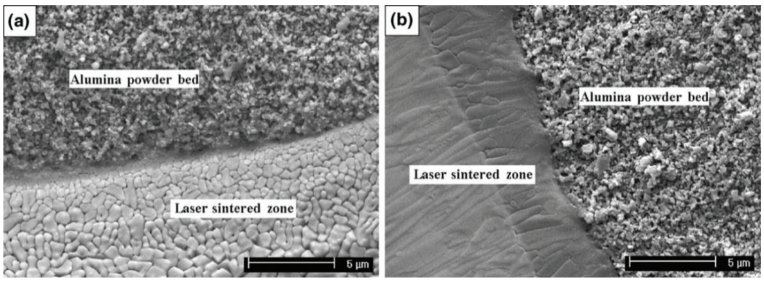

Figure 9. SEM micrographs of powder beds densified using laser scanning speeds of (a) 4 mm/s and (b) 2 mm/s. Reprinted from [27], with permission of Elsevier.

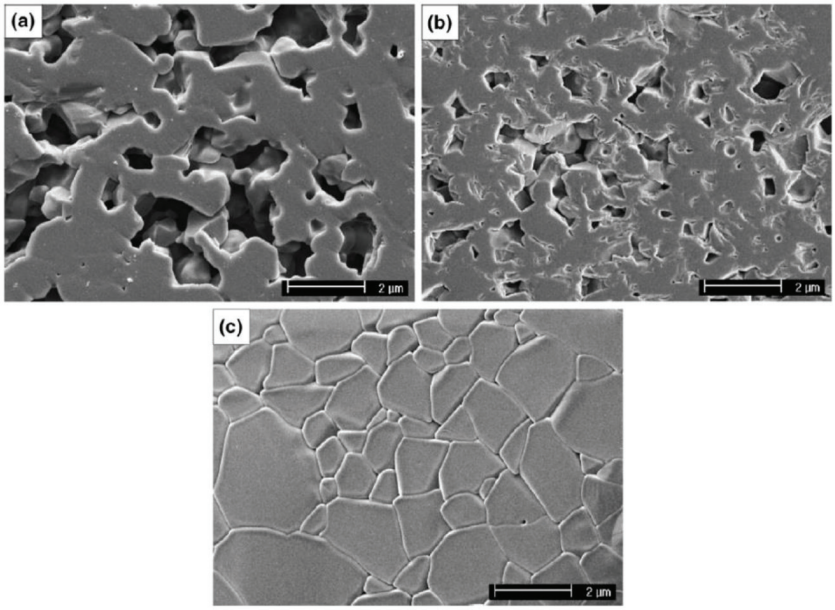

Figure 10. Cross-section SEM micrographs of alumina powder beds densified using laser energy densities of (a) 4.0 J mm^{-2} (b) 7.0 J mm^{-2} and (c) 8.5 J mm^{-2}. Reprinted from [27], with permission of Elsevier.

avoid large grain size and high thermal gradients. A relatively high density of 85% was obtained after the post-process heating.

Wu et al. also applied a CO_2 laser to process 99.8 wt.% pure alumina [27]. The special treatment here is that the fine particles (0.45 μm) of the alumina powder beds were generated through aerosol assisted spray deposition. The study clearly demonstrated the effect of scanning speed (**Figure 9**) and laser energy density (**Figure 10**) on the microstructure of the laser-sintered alumina powder beds. A higher laser power, a lower laser scanning speed or a smaller

laser beam size resulted in a higher laser energy density, and the resulting higher temperature promoted the densification of the powder bed. By increasing the energy density, the microstructure of the powder beds varied from open pores to full densification.

4.2. Exemplar II: Silica (SiO_2)

Silicon dioxide, also known as silica, is one of the most common ceramic materials. As the major constituent of sand, it is very abundant. Silica is widely used as structural materials, in microelectronics, and in food and pharmaceutical industries due to varies properties such as high melting temperature and very low thermal and electrical conductivity. Most silica is produced by mining such as sand mining and purification of quartz. Silica parts can be laser processed by direct or indirect method.

Yap et al. demonstrated the SLM process using a short wavelength laser. They reported complete melting and forming a 100 μm thick layer of 99.7% pure silica powder in Ar through a good combination of parameters even at very low optical absorption (0.04 for SiO_2 @ 1.06 μm) [58]. The laser energy density was between 16.7 and 25 J/mm^{2***}. They also showed that sunken cores formed from high laser energy density, suggesting vaporization of silica material during the process.

Lee et al. showed the indirect SLS process on a slurry-deposited layer. They reported successful sintering slurry of silica powder (60 wt.%) and silica sol (40 wt.%) with a small energy density using a CO_2 laser [57]. They also demonstrated a better surface finish and a good edge profile with a proper laser energy density feedback control process.

The following two examples show the direct SLS process, and the relation between laser processing parameters and the surface roughness and dimensional accuracy of the sintered parts. Wang et al. made use of a CO_2 laser to directly sinter silica sand, which is a mixture of SiO_2 (97.51 wt.%), with small amount of a variety of impurity of elements such as Zr, Ti, Ca, Al, Ba, Fe, Cs, Mg [11]. Pure silica softens at 1500°C and melts at 1600°C [11], but the impurities form a low-melting point eutectic that partially melts at 500–700°C. The existence of impurities

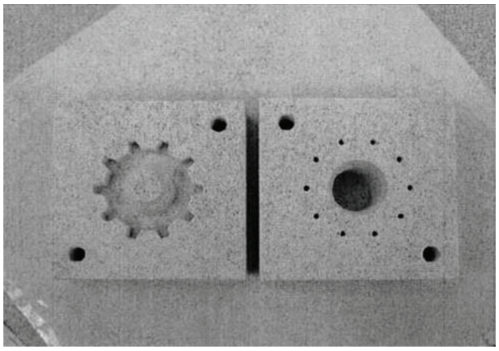

Figure 11. Sand mold built from silica sand powders, using LPBF. Reprinted from [11], with permission of Springer.

therefore facilitates the direct laser sintering of the silica sand. Wang et al. studied the influence of the laser process parameters and concluded that larger power and a smaller scanning speed led to greater strength and thickness, but the process also produced a rough surface finish. To improve the surface conditions, instead of a common polishing process, a simple infiltration post-process improved the roughness of the horizontal surface from R_a = 35.6–25.4 μm. One example of the directly sintered parts in silica sand is shown in **Figure 11**.

Tang et al. also directly sintered silica sand with a CO_2 laser [68] and preheated the powder bed up to 400°C. The silica sand consisted mainly of SiO_2 with a very low percentage of Al_2O_3, and the small amount of Al_2O_3 acted with SiO_2 to form a low-melting-point eutectic. This eutectic facilitated the melting of the surface of the sand particles under laser heating, although the core of the particle remained at the high melting point. The sand particles bound together through the liquid surfaces when the laser beam struck and then quickly solidified after the laser beam moved away. Tang et al. further studied how the process parameters affected the properties of the laser sintered parts and concluded the compression strength of the products increased when the laser power increased and decreased when the scanning speed increased. The largest compression strength they produced was 15.5 MPa with a laser power of 120 W and a scanning speed of 60 mm/s. They also found the surface roughness of sintered products increased when the laser power increased and decreased when the scanning speed increased. The smallest surface roughness they achieved was R_a = 19 μm at the laser power of 120 W and the scanning speed of 180 mm/s. Finally, the absolute errors (the differences from the actual sizes of sintered parts to the design sizes) ranged from 0.1 to 0.5 mm, depending on the laser process parameters. The best result (0.137 mm in the *x* direction and 0.117 mm in the *y* direction) was achieved when both the laser power (160 W) and the scanning speed (180 mm/s) were the largest among the parameters they tested. However, the researchers also found the dimensional accuracy of the sintered parts was relatively stable and insensitive to a certain range of processing parameters.

Liu et al. exhibited the indirect SLS process with a short wavelength laser, and it also showed the relation between laser line energy and porosity, mechanical strength, and shrinkage depth of the manufactured parts. They reported the indirect laser sintering on polymer coated silica sand composite powders using a 1.064 μm laser [46]. The silica sand they used mainly consisted of SiO_2 99%, Al_2O_3 0.22% and micro-content of TiO_2 with a melting point of 1750°C [46]. The silica sand was coated with 1.9-2.1 wt.% of phenol-formaldehyderesin (PF). Liu et al. studied the relation between line energy (power/scanning speed) and properties of the sintered parts. The best line energy was located between 10 and 20 J/m, which resulted in a porosity of 29–32% for the laser sintered parts. Both the porosity and shrinkage depth of the powder bed generally increased with the increase of the line energy in that range, while the shrinkage depth gradually fell after 20 J/m. With a set of optimized parameters (laser power of 7 W, scanning speed of 400 mm/s, and laser beam spot of 50 μm), a compressive strength of 0.8 MPa was obtained. This strength was equivalent to that of sand patterns made by the common method and exhibiting strengths in the range 0.5–2.5 MPa [46].

Song et al. demonstrated the indirect SLS process with a long wavelength laser, and they showed the relation between laser process parameter and the dimensional accuracy of the

fabricated parts. They indirectly sintered PF/silica sand compounds using a CO_2 laser [52]. They found laser process parameters had important effects on the property and accuracy of the sintered parts. For example, the scanning speed affected the size of the sintered parts: with an increase of the scanning speed from 5 mm/s to 13.3 mm/s, the dimensions of the sintered sample shrank for about 1.5 mm in both length and height, and 1 mm in width.

4.3. Exemplar III: Mixture of oxide ceramics

The following example shows the effect of laser energy density and layer thickness to the mechanical properties of the produced part. Silica can be used as bio-ceramics for tissue scaffolds or dental implants when it is mixed with other ceramics or minerals, such as hydroxyapatite (HA), feldspar, kaolin and alumina [58]. F.-H. Liu performed selective laser sintering on hydroxyapatite-silicate slurry with a CO_2 laser [8]. The mixture was comprised of SiO_2-P_2O_5-CaO, materials which had the potential to produce bone scaffolds for tissue engineering applications. An optimized laser energy density was critical to the process. An energy density that was too small would result in an overlap between layers less than 15%, which led to insufficient bonding strength. An excessive energy density would result in warping layers if the overlap exceeds 30%. With an optimized slurry (28 wt.% SiO_2, 30 wt.% HA, and 42 wt.% H_2O), a laser energy density of less than 1 J/mm^2 enabled formation of the bio-ceramic parts. The paper further revealed the significant effect of laser energy density on bending strength, as shown in **Figure 12**. The maximum strength achieved was 4.7 MPa at 1.6 J/mm^2.

The following example exhibited the indirect SLS process and the effect of the laser process parameters. The mixture K_2O-Al_2O_3-SiO_2 shows excellent mechanical properties and biocompatibility which come up to the ISO standards as a dental restoration material [70, 71]. Liu et al.

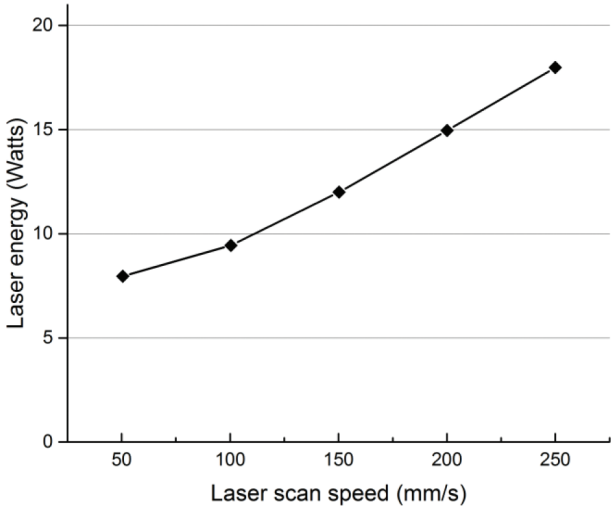

Figure 12. Relationship between laser scanning speed and laser energy. The data presented here are extracted from those presented in the original source [8].

studied the composite powder of an epoxy resin binder E-12 and K_2O-Al_2O_3-SiO_2 series of dental glass-ceramics through indirect selective laser sintering [59]. The paper described the effect of the laser processing parameters on the relative density of the sintered parts and concluded that laser power, scan spacing, and scanning speed had different effects to the produced part. Specifically, the factor of laser power had the greatest ability to influence the relative density and the bending strength, the factor of scanning speed had the least effects, and the factor of scan spacing was in between. In order to obtain high density parts, they suggested increasing the laser power and decreasing the scan spacing and the scanning speed. However, the authors suggest other factors such as SLS forming efficiency and forming precision should also be considered for optimizing the processing parameters [59]. An example of the processing parameters and the parts' properties is illustrated in **Table 6**. The bending strength was basically proportional to the relative density of the sintered parts. Although in general the relative density followed the laser energy density, this relationship was only approximate. For example, sample numbers 1, 4, and 7 had the same energy density but different relative density and mechanical properties. The paper also noted that the preheating temperature was an important processing parameter that affected the viscous binder's wetting and spreading characteristics, so it had a considerable influence on the relative density of the sintered parts. The optimized processing parameters, the preheating temperature, the laser power, the scanning speed, the scan spacing and the layer thickness were 30–35°C, 21 W, 1800 mm/s, 100 and 80 μm, respectively. Under such conditions, the relative density and bending strength reached 37.40% and 2.08 MPa, respectively. An example of the indirectly sintered glass-ceramic part is shown in **Figure 13**.

For component mixed ceramic materials, it is common to use additive elements to bind them before the LPBF process. However, a pure mixture without a binder is possible to be processed. For example, Bertrand et al. showed a direct process on pure yttria-zirconia (Y_2O_3-ZrO_2) powders through selective laser sintering/melting using a 1.064 μm fiber laser [12]. The authors studied the influence from the powder and the powder bed and found the properties

No.	Laser power (W)	Scan speed (mm/s)	Scan spacing (mm)	Energy density (J/mm^2)	Relative density (%)	Bending strength σ_{fM} (MPa)
1	15	1600	0.10	0.0938	34.59	1.63
2	15	1800	0.12	0.0694	33.79	1.59
3	15	2000	0.14	0.0536	33.70	1.54
4	18	1600	0.12	0.0938	34.83	1.66
5	18	1800	0.14	0.0714	33.98	1.62
6	18	2000	0.10	0.0900	35.05	1.98
7	21	1600	0.14	0.0938	36.59	2.01
8	21	1800	0.10	0.1167	37.40	2.08
9	21	2000	0.12	0.0875	36.38	2.02

Table 6. SLS results for dental glass-ceramic powder. The data presented here are from those presented in the original source [59].

Figure 13. Teeth made by SLS under the optimized technical parameters Reprinted from [59], with permission of Emerald Publishing Limited.

of particles and powder layers significantly affected the product. For example, they found the best powder for the fiber laser to process was a powder in which all particles have a diameter less than 1 μm. Atomized powders helped to avoid electrostatic charges that led to powder agglomeration. Furthermore, the particle morphology directly affected the powder spreading and the powder bed density in that the more spherical particles improved the results although the authors of the work did not specify the aspects which were improved. The layer thickness is a crucial parameter for a good sintering/melting process. To decide this parameter, the paper suggested that the laser had to penetrate at least through the last powder layer and the previous one. Earlier, Wilkes and Wissenbach suggested that the layer thickness needs to be 10 times greater than the particle size for achieving efficient roller powder layering [61]. To satisfy these requirements, Bertrand et al. reported a 30 μm thick layer in their study. The paper also reported the preheating effect and concluded that, on one hand, the preheating reduced the micro cracks; on the other hand, preheating decreased powder flowability and impaired process repeatability. An example from such a direct laser process is shown in **Figure 14**.

The following discussion shows the effect of preheating and the secondary laser assistance. Oxide ceramics such as zirconia and alumina are widely used in industry and in medical applications such as bearing sleeves and valves, high density grinding media, cutting blades, crowns and bridges in dental restorations. Hagedorn et al. reported direct selective laser melting on an eutectic Al_2O_3-ZrO_2-Y_2O_3 mixture without any binder materials [48, 54]. The mixture was composed of 58.5 wt.% of Al_2O_3 (melting point 2072°C) and 41.5 wt.% ZrO_2 (melting point 2710°C) where ZrO_2 contains 6 wt.% yttria (Y_2O_3) to form a eutectic powder. It demonstrated a complete melting to the ceramic powders using a low optical absorptive Nd: YAG laser with a wavelength of 1.06 μm. The unique feature here is the work applied a CO_2 laser assistant that preheated the powder bed surface above 1600°C, very close to the eutectic mixture melting point of 1860°C. The secondary laser helped to reach the melting temperature of the ceramics and led to a large melting pool. Such a process improved the density of the obtained part. For example, with the optimized process parameters, the laser processed part

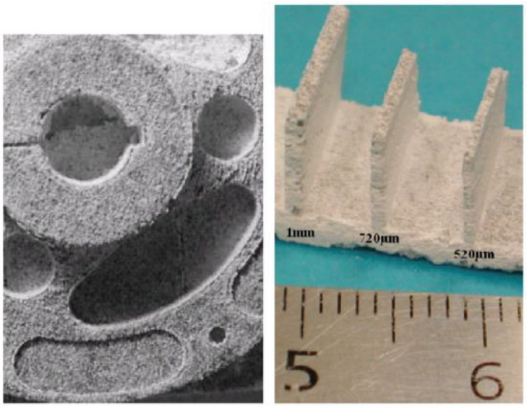

Figure 14. Pure zirconia 3D objects manufactured by SLS/M technology Reprinted from [12], with permission of Elsevier.

yielded a relative density of approximately 100% without any post-processing. Such a part showed a fine-grained nano-sized microstructure and flexural strengths of above 500 MPa, sufficient for dental restorations. This value is in the same range but at the lower end compared with conventionally manufactured parts which have flexural strengths of 800–1200 MPa for zirconia [72], 400 MPa for alumina [73] and 480–2400 MPa for mixtures of zirconia and alumina [9, 74]. On the other hand, the second laser assistance negatively affected the surface quality and dimensional accuracy because the low viscosity melt pool flowed outside the boundaries of the scanned part and wet the surrounding powders. The surface roughness was R_z ~ 100 μm, one of the best in SLM-processed high-strength oxide ceramics. The dimensional accuracy reached ~150 μm, which was far below that of the conventionally milled parts of ~50 μm. An example of a direct SLM produced full ceramic framework for a dental restoration is shown in **Figure 15**. A rough surface may induce stress peaks on mechanical loading, which leads to premature failure and thus affects the mechanical strength. The preheating

Figure 15. Direct SLM produced full ceramic framework for a dental restoration Reprinted from [54], with permission of Elsevier.

method may also induce thermal shocks during the deposition of the cold ceramic powder, which can result in fine cracks on the surface of the produced part and hence reduce the mechanical strength, as shown in **Figure 16**.

The following example showed the effect of particle shapes. Wilkes et al. [9] used the same setups from Refs. [48, 54]. The authors studied how the particle shape (spherical vs. irregular) affected the manufactured parts, and found it had a strong influence on the relative density of the SLM produced parts. There was a significant improvement of the porosity and relative density which was most likely due to the better flowability of spherically shaped particles compared to irregularly shaped particles. A parallel comparison of two cross-sections using different shaped powders is shown in **Figure 17**. The paper described the effect of preheating and concluded temperature differences and gradients during SLM were reduced through the preheating process. Therefore, mechanical stresses were significantly reduced, and large crack formation could be avoided. As reported in Refs. [48, 54], fine cracks can still be found for building up large parts because of the local rapid cooling from the deposition of the cold powder layers on top of the preheated ceramic. The preheated zone in the SLM machine is shown in **Figure 18**. A comparison of the product surface without preheating and with preheating at 1715°C is shown in **Figure 19**.

Shishkovsky et al. showed the effect of an oxygen-deficit environment. They performed alumina-zirconium ceramics synthesis through selective laser sintering/melting [13]. The ceramic mixture was composed of yttria-stabilized zirconia, called YSZ (ZrO_2 90 wt.%, Y_2O_3 10 wt.%), and aluminum or alumina Al_2O_3 in the ratio 4:1. They investigated the influence of SLS/SLM processing in air or in a protective gas environment. Laser sintering in argon required scan velocities nearly one order of magnitude smaller than velocities when sintering in air, and the surface temperature of the powder bed was much lower in argon, as well. The thickness of one layer that was sintered in one cycle increased by 1.5–2 times, so the energy needed for sintering in argon gas was much smaller than that in air. When operating in air, they also observed strong sparkling and scattering of the powder material from the interaction

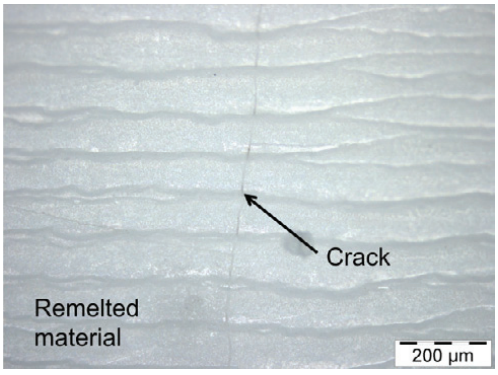

Figure 16. Crack formation on the surface of the SLM part due to cold powder deposition onto the preheated area Reprinted from [54], with permission of Elsevier.

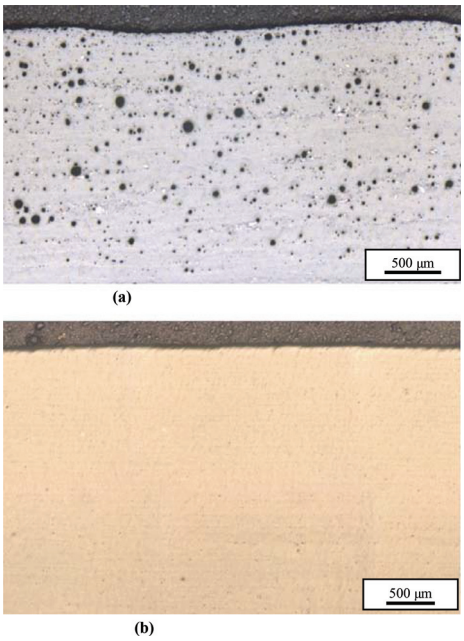

Figure 17. Cross-sections of two specimens made using different types of powder (a) irregular shaped powder particles (b) spherical powder particles. Reprinted from [9], with permission of Emerald Publishing Limited.

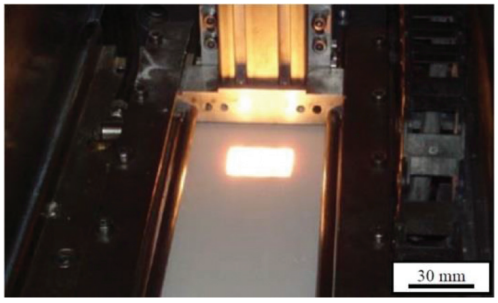

Figure 18. Photo of the preheated zone in the SLM machine. Reprinted from [9], with permission of Emerald Publishing Limited.

zone beyond a certain energy density. SLS in air yields ceramics with a dense structure and a uniform distribution of the stabilizing phases although cracks could happen at high laser powers during high-speed cooling. While sintering in argon, a porous part was developed with pore size >100 μm, and the pore shape was elongated in the laser scan direction. Such a high porosity greatly reduced the relative density and the mechanical strength of the sintered ceramics. The surface comparison of the ceramics sintered in air and in argon is shown in **Figure 20**. The research also compared the SLS and SLM processes and demonstrated that

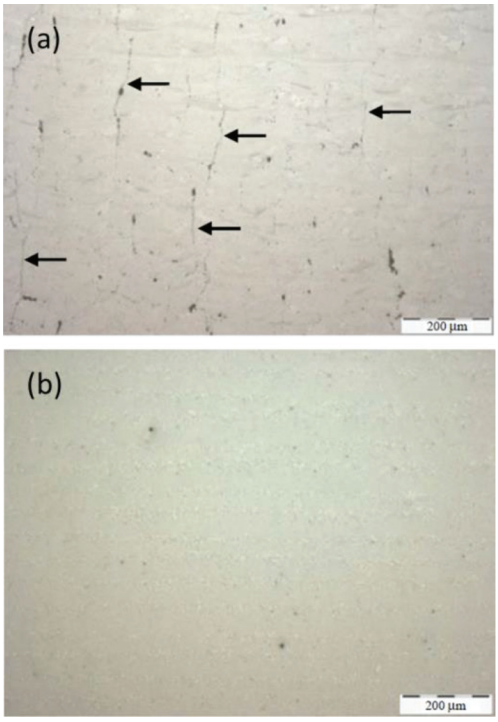

Figure 19. Cross-sections of specimens manufactured by SLM (a) cracks formation without preheating and (b) crack-free with preheating at 1715°C. Reprinted from [9], with permission of Emerald Publishing Limited.

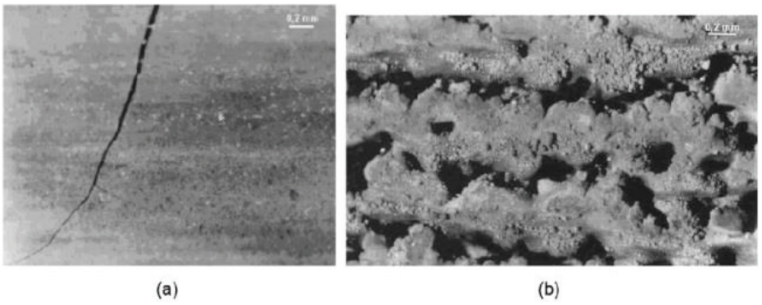

Figure 20. Surface comparison of the sintered YSZ-Al/Al_2O_3 at P = 24.1 W, V = 3.1 cm/s. Magnification: (a) 50× (in air) and (b) 20× (in argon). Reprinted from [13], with permission of Elsevier.

SLM allows for manufacturing objects with a relatively low porosity and a high geometrical accuracy. Examples of the ceramics manufactured from SLS and SLM techniques are shown in **Figure 21**. The surface porosity appeared to increase by increasing the laser scan velocity and the hatch distance.

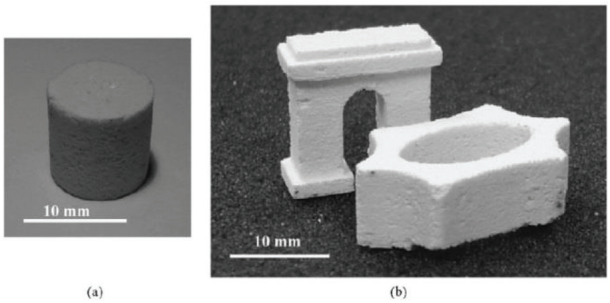

Figure 21. Manufactured ceramic objects: (a) porous filter element from corundum–zirconium ceramics produced by SLS process; (b) samples produced by SLM process from ZrO_2 powder. Reprinted from [13], with permission of Elsevier.

5. Perspectives

Comparing to metals, laser powder bed fusion of ceramics is relatively new, less studied, and less mature [21, 75–77]. Ceramics are a large materials family which includes oxides (Al_2O_3, MgO, ZrO_2, FeO, NiO, SiO_2, CuO, $Ca_3(PO_4)_2$, etc.), carbides (BC, SiC, WC, etc.), nitrides (Si_3N_4, $Al_6N_6O_2Si$, AlN, etc.), sulfides (Yb_3S_4, CeS, $CaLa_2S_4$, $MgYb_2S_4$, $MnEr_2S_4$, $ZnGa_2S_4$, etc.), fluorides (CaF_2, BaF_2, SrF_2, etc.), and ceramic component mixtures (Al_2O_3-ZrO_2, Al_2O_3-SiO_2, ZrO_2-Y_2O_3, Li_2O-Al_2O_3-SiO_2, K_2O-Al_2O_3-SiO_2, etc.). However, so far the laser powder bed fusion on ceramics has been studied on only a small fraction of this materials family. Not all of them may be suitable for the current layer-by-layer construction technique due to factors such as high melting temperature, different optical/thermal properties, or availability of suitable powders. Further development may lead to construction of multi-material, multifunctional objects.

To obtain desired structural and physical properties of a fabricated part, an optimized process is required for the laser powder bed fusion technique. However, since the process parameters are completely material-dependent and can be varied largely for different ceramics, it is necessary to optimize the process parameters for each material through series of experiments, theoretical modeling, or a combination of both. The optimization includes powder, laser, and environmental factors, as well as possible pre- and post-processes.

In recent years, new development has been focused on using the laser powder bed fusion technique for different ceramic materials and application of the manufactured parts in various industrial and medical fields. However, detailed process-structure studies are still missing. It is critical to investigate the material' microstructure and the physical properties of the ceramic parts made from laser powder bed fusion. It is therefore necessary to explore the relation among the process parameters, the size, shape, and boundary conditions of the laser-fused micro-grains, and the macro-properties of the fabricated part. Such study will increase the understanding of the laser powder bed fusion technique from the micro- to the meso-scale.

6. Conclusion

Laser powder bed fusion enables the production of ceramic parts with very high temperatures and excellent precision in a short time. The process is suitable for processing hard materials with complex geometries. However, due to several intrinsic properties, the LPBF technique for ceramics is far from mature and is still in the research and development phase. Limiting factors include susceptibility to thermal stresses, low fracture toughness, and low optical absorptivity in the near-infrared region for oxide ceramics. As these factors are further investigated, the difficulties related to them may be solved. For example, proper choice of lasers and powders, combined with an optimum process, can compensate for or overcome some of the limitations and produce near 100% relative density. Such near pore-free parts have only micro-cracks or no cracks, and their mechanical properties are close to those manufactured from conventional methods. The LPBF technique therefore shows potential for ceramic fabrication and will continue to attract research and industrial interests in the future.

Author details

Haidong Zhang* and Saniya LeBlanc*

*Address all correspondence to: haidongzhang@gmail.com and sleblanc@gwu.edu

Department of Mechanical and Aerospace Engineering, The George Washington University, Washington, DC, USA

References

[1] Kruth J, Mercelis P, Van Vaerenbergh J, Froyen L, Rombouts M. Binding mechanisms in selective laser sintering and selective laser melting. Rapid Prototyping Journal. 2005;**11**(1): 26-36. DOI: 10.1108/13552540510573365

[2] Deckard CR. Method and apparatus for producing parts by selective sintering [Internet]. US; US4863538 A. 1986. Available from: https://www.google.com/patents/US4863538

[3] Deckard CR, Beaman JJ, Darrah JF. Method for selective laser sintering with layerwise cross-scanning [Internet]. US; US5155324 A. 1992. Available from: https://www.google.com/patents/US5155324

[4] Meiners W, Wissenbach K, Gasser A. Selective laser sintering at melting temperature [Internet]. US6215093 B1. 1996. Available from: https://www.google.com/patents/US6215093

[5] El-Desouky A, Carter, Andre MA, Bardet PM, LeBlanc S. Rapid processing and assembly of semiconductor thermoelectric materials for energy conversion devices. Materials Letters. 2016;**185**:598-602. DOI: 10.1016/J.MATLET.2016.07.152

[6] El-Desouky A, Carter M, Mahmoudi M, Elwany A, LeBlanc S. Influences of energy density on microstructure and consolidation of selective laser melted bismuth telluride thermoelectric powder. Journal of Manufacturing Processes. 2017;**25**:411-7. DOI: 10.1016/J.JMAPRO.2016.12.008

[7] Deckers J, Vleugels J, Kruth J-P. Additive manufacturing of ceramics: A review. Journal of Ceramic Science and Technology. 2014;**5**(4):245-260. DOI: 10.4416/JCST2014-00032

[8] Liu F-H. Synthesis of bioceramic scaffolds for bone tissue engineering by rapid prototyping technique. Journal of Sol-Gel Science and Technology. 2012;**64**(3):704-710. DOI: 10.1007/s10971-012-2905-5

[9] Wilkes J, Hagedorn Y, Meiners W, Wissenbach K. Additive manufacturing of ZrO_2-Al_2O_3 ceramic components by selective laser melting. Rapid Prototyping Journal. 2013;**19**(1):51-57. DOI: 10.1108/13552541311292736

[10] Ferrage L, Bertrand G, Lenormand P, Grossin D, Ben-Nissan B. A review of the additive manufacturing (3DP) of bioceramics: Alumina, zirconia (PSZ) and hydroxyapatite. Journal of the Australian Ceramic Society. 2017;**53**(1):11-20. DOI: 10.1007/s41779-016-0003-9

[11] Wang XH, Fuh JYH, Wong YS, Tang YX. Laser sintering of silica sand—Mechanism and application to sand casting mould. International Journal of Advanced Manufacturing Technology. 2003;**21**(12):1015-1020. DOI: 10.1007/s00170-002-1424-x

[12] Bertrand P, Bayle F, Combe C, Goeuriot P, Smurov I, Titov VI. Ceramic components manufacturing by selective laser sintering. Applied Surface Science. 2007;**254**(4):989-992. DOI: 10.1016/j.apsusc.2007.08.085

[13] Shishkovsky I, Yadroitsev I, Bertrand P, Smurov I. Alumina–zirconium ceramics synthesis by selective laser sintering/melting. Applied Surface Science. 2007;**254**(4):966-970. DOI: 10.1016/j.apsusc.2007.09.001

[14] Yeong W, Yap C, Mapar M, Chua C. State-of-the-art review on selective laser melting of ceramics. In: Bártolo P, Lemos A, Pereira A, Mateus A, Ramos C, Santos C, et al., editors. High Value Manufacturing: Advanced Research in Virtual and Rapid Prototyping [Internet]. Boca Raton, FL: CRC Press; 2013. pp. 65-70. DOI: 10.1201/b15961-14

[15] Dalgarno KW, Wright CS. Approaches to processing metals and ceramics through the laser scanning of powder beds—A review. Powder Metallurgy Progress. 2001;**1**(1):70-79. Available from: http://www.imr.saske.sk/pmp/issue/1-2001/PMP_Vol01_No1_p070-079.pdf

[16] Sigmund WM, Bell NS, Bergström L. Novel powder-processing methods for advanced ceramics. Journal of the American Ceramic Society. 2004;**83**(7):1557-1574. DOI: 10.1111/j.1151-2916.2000.tb01432.x

[17] Samant AN, Dahotre NB. Laser machining of structural ceramics—A review. Journal of the European Ceramic Society. 2009;**29**(6):969-993. DOI: 10.1016/J.JEURCERAMSOC.2008.11.010

[18] Wong KV, Hernandez A. A review of additive manufacturing. ISRN Mechanical Engineering. 2012;**2012**:1-10. DOI: 10.5402/2012/208760

[19] Qian B, Shen Z. Laser sintering of ceramics. Journal of Asian Ceramic Societies. 2013;**1**(4):315-321. DOI: 10.1016/J.JASCER.2013.08.004

[20] Shirazi SFS, Gharehkhani S, Mehrali M, Yarmand H, Metselaar HSC, Adib Kadri N, et al. A review on powder-based additive manufacturing for tissue engineering: Selective laser sintering and inkjet 3D printing. Science and Technology of Advanced Materials. 2015; **16**(3):33502. DOI: 10.1088/1468-6996/16/3/033502

[21] Yap CY, Chua CK, Dong ZL, Liu ZH, Zhang DQ, Loh LE, et al. Review of selective laser melting: Materials and applications. Applied Physics Reviews. 2015;**2**(4):41101. DOI: 10.1063/1.4935926

[22] Hegab HA. Design for additive manufacturing of composite materials and potential alloys: A review. Manufacturing Review. 2016;**3**:11. DOI: 10.1051/mfreview/2016010

[23] Sing SL, Yeong WY, Wiria FE, Tay BY, Zhao Z, Zhao L, et al. Direct selective laser sintering and melting of ceramics: A review. Rapid Prototyping Journal. 2017;**23**(3):611-623. DOI: 10.1108/RPJ-11-2015-0178

[24] Kruth JP, Wang X, Laoui T, Froyen L. Lasers and materials in selective laser sintering. Assembly Automation. 2003;**23**(4):357-371. DOI: 10.1108/01445150310698652

[25] Tian X, Sun B, Heinrich JG, Li D. Scan pattern, stress and mechanical strength of laser directly sintered ceramics. International Journal of Advanced Manufacturing Technology. 2013;**64**(1–4):239-246. DOI: 10.1007/s00170-012-3994-6

[26] Triantafyllidis D, Li L, Stott FH. Investigation of the effects of nonconventional beam geometries in laser surface treatment of ceramics: Experimental analysis. Journal of Laser Applications. 2006;**18**(3):267-274. DOI: 10.2351/1.2193522

[27] Wu Y, Du J, Choy K-L, Hench LL. Laser densification of alumina powder beds generated using aerosol assisted spray deposition. Journal of the European Ceramic Society. 2007;**27**(16):4727-4735. DOI: 10.1016/J.JEURCERAMSOC.2007.02.219

[28] Juste E, Petit F, Lardot V, Cambier F. Shaping of ceramic parts by selective laser melting of powder bed. Journal of Materials Research. 2014;**29**(17):2086-2094. DOI: 10.1557/jmr.2014.127

[29] Murali K, Chatterjee AN, Saha P, Palai R, Kumar S, Roy SK, et al. Direct selective laser sintering of iron–graphite powder mixture. Journal of Materials Processing Technology. 2003;**136**(1–3):179-185. DOI: 10.1016/S0924-0136(03)00150-X

[30] Simchi A. Direct laser sintering of metal powders: Mechanism, kinetics and microstructural features. Materials Science and Engineering A. 2006;**428**(1–2):148-158. DOI: 10.1016/J.MSEA.2006.04.117

[31] Kruth J-P, Levy G, Klocke F, Childs THC. Consolidation phenomena in laser and powder-bed based layered manufacturing. CIRP Annals. 2007;**56**(2):730-759. DOI: 10.1016/J.CIRP.2007.10.004

[32] Levy GN, Schindel R, Kruth JP. Rapid manufacturing and rapid tooling with layer manufacturing (lm) technologies, state of the art and future perspectives. CIRP Annals. 2003;**52**(2):589-609 DOI: 10.1016/S0007-8506(07)60206-6

[33] Glardon R, Karapatis N, Romano V, Levy GN. Influence of Nd:YAG parameters on the selective laser sintering of metallic powders. CIRP Annals. 2001;**50**(1):133-136. DOI: 10.1016/S0007-8506(07)62088-5

[34] Shao TM, Lin XC, Zhou M. bsorption of some powder materials to YAG laser. Science in China (Series A). 2001;**44(**Suppl.):489-94. Available from: http://www.scichina.com:8081/sciAe/fileup/PDF/01ya0489.pdf

[35] Pham DT, Dimov SS, Petkov PV. Laser milling of ceramic components. International Journal of Machine Tools and Manufacture. 2007;**47**(3–4):618-626. DOI: 10.1016/j.ijmachtools.2006.05.002

[36] Deckers J, Shahzad K, Vleugels J, Kruth JP. Isostatic pressing assisted indirect selective laser sintering of alumina components. Rapid Prototyping Journal. 2012;**18**(5):409-419. DOI: 10.1108/13552541211250409

[37] Hellrung D, Yeh L-Y, Depiereux F, Gillner A, Poprawe R. High-accuracy micromachining of ceramics by frequency-tripled Nd:YAG lasers. Proc SPIE 1999;**3618**:348–356. DOI: 10.1117/12.352697

[38] Prashanth KG, Scudino S, Maity T, Das J, Eckert J. Is the energy density a reliable parameter for materials synthesis by selective laser melting? Materials Research Letters. 2017;**5**(6):386-390. DOI: 10.1080/21663831.2017.1299808

[39] Tolochko NK, Khlopkov YV, Mozzharov SE, Ignatiev MB, Laoui T, Titov VI. Absorptance of powder materials suitable for laser sintering. Rapid Prototyping Journal. 2000;**6**(3):155-161. DOI: 10.1108/13552540010337029

[40] Li R, Liu J, Shi Y, Wang L, Jiang W. Balling behavior of stainless steel and nickel powder during selective laser melting process. International Journal of Advanced Manufacturing Technology. 2012;**59**(9–12):1025-1035. DOI: 10.1007/s00170-011-3566-1

[41] Das S. Physical aspects of process control in selective laser sintering of metals. Advanced Engineering Materials. 2003;**5**(10):701-711. DOI: 10.1002/adem.200310099

[42] Tolochko NK, Mozzharov SE, Yadroitsev IA, Laoui T, Froyen L, Titov VI, et al. Balling processes during selective laser treatment of powders. Rapid Prototyping Journal. 2004;**10**(2):78-87. DOI: 10.1108/13552540410526953

[43] Ho HCH, Gilbson I, Cheung WL. Effects of energy density on morphology and properties of selective laser sintered polycarbonate. Journal of Materials Processing Technology. 1999;**89–90**:204-210. DOI: 10.1016/S0924-0136(99)00007-2

[44] Beaman JJ, Barlow JW, Bourell DL, Crawford RH, Marcus HL, McAlea KP. Solid Freeform Fabrication: A New Direction in Manufacturing [Internet]. Springer US: Boston, MA; 1997. Available from: http://link.springer.com/10.1007/978-1-4615-6327-3

[45] Ciurana J, Hernandez L, Delgado J. Energy density analysis on single tracks formed by selective laser melting with CoCrMo powder material. International Journal of Advanced Manufacturing Technology. 2013;**68**(5–8):1103-1110. DOI: 10.1007/s00170-013-4902-4

[46] Liu FR, Zhao JJ, Zhang Q, He C, Chen JM. Processing and characterizations of 2%PF/silica sand core–shell composite powders by selective laser sintering with a higher transmittance fiber laser. International Journal of Machine Tools and Manufacture. 2012;**60**:52-58. DOI: 10.1016/J.IJMACHTOOLS.2012.05.003

[47] Syrjälä S, Tuomi J. Rapid prototyping: Mallien, prototyyppien ja työkalujen pikavalmistus [Internet]. Tekes; 1997. (Teknologiakatsaus/Teknologian kehittämiskeskus TEKES). Available from: https://hamk.finna.fi/Record/vanaicat.41156

[48] Hagedorn Y-C, Balachandran N, Meiners W, Wissenbach K, Poprawet R. SLM of net-shaped high strength ceramics: New opportunities for producing dental restorations. In: SFF Symposium [Internet]. Austin, TX, USA: University of Texas at Austin; 2011. Available from: https://sffsymposium.engr.utexas.edu/Manuscripts/2011/2011-42-Hagedorn.pdf

[49] Liu LX, Marziano I, Bentham AC, Litster JD, White ET, Howes T. Effect of particle properties on the flowability of ibuprofen powders. International Journal of Pharmaceutics. 2008; **362**(1–2):109-117. DOI: 10.1016/j.ijpharm.2008.06.023

[50] Gibson I, Shi D. Material properties and fabrication parameters in selective laser sintering process. Rapid Prototyping Journal. 1997;**3**(4):129-136. DOI: 10.1108/13552549710191836

[51] Gusarov AV, Yadroitsev I, Bertrand P, Smurov I. Heat transfer modelling and stability analysis of selective laser melting. Applied Surface Science. 2007;**254**(4):975-979. DOI: 10.1016/J.APSUSC.2007.08.074

[52] Song JL, Li YT, Deng QL, Hu DJ. Rapid prototyping manufacturing of silica sand patterns based on selective laser sintering. Journal of Materials Processing Technology. 2007;**187–188**: 614-618. DOI: 10.1016/J.JMATPROTEC.2006.11.108

[53] Joguet D, Costil S, Liao H, Danlos Y. Porosity content control of CoCrMo and titanium parts by Taguchi method applied to selective laser melting process parameter. Rapid Prototyping Journal. 2016;**22**(1):20-30. DOI: 10.1108/RPJ-09-2013-0092

[54] Hagedorn Y-C, Wilkes J, Meiners W, Wissenbach K, Poprawe R. Net shaped high performance oxide ceramic parts by selective laser melting. Physics Procedia. 2010;**5**:587-594. DOI: 10.1016/j.phpro.2010.08.086

[55] Deckers J, Meyers S, Kruth JP, Vleugels J. Direct selective laser sintering/melting of high density alumina powder layers at elevated temperatures. Physics Procedia. 2014;**56**:117-124. DOI: 10.1016/J.PHPRO.2014.08.154

[56] Wang Z, Shi Y, He W, Liu K, Zhang Y. Compound process of selective laser processed alumina parts densified by cold isostatic pressing and solid state sintering: Experiments, full process simulation and parameter optimization. Ceramics International. 2015;**41**(2): 3245-3253. DOI: 10.1016/j.ceramint.2014.11.014

[57] Lee RT, Liu FH, Ting KE, Yeh SL, Lin WH. Laser compensation for ceramics accuracy improvement of selective laser sintering. Advances in Materials Research. 2014;**902**:12-17. DOI: 10.4028/WWW.SCIENTIFIC.NET/AMR.902.12

[58] Yap C, Chua C, Dong Z, Liu Z, Zhang D. Single track and single layer melting of silica by Selective Laser Melting. In: Bártolo P, Lemos A, Pereira A, Mateus A, Ramos C, Santos C, et al., editors. High Value Manufacturing: Advanced Research in Virtual and Rapid Prototyping [Internet]. Boca Raton, FL: CRC Press; 2013. pp. 261-5. DOI: 10.1201/b15961-49

[59] Liu J, Zhang B, Yan C, Shi Y. The effect of processing parameters on characteristics of selective laser sintering dental glass-ceramic powder. Rapid Prototyping Journal. 2010;**16**(2):138-145. DOI: 10.1108/13552541011025861

[60] Bertoli US, Wolfer AJ, Matthews MJ, Delplanque J-PR, Schoenung JM. On the limitations of volumetric energy density as a design parameter for selective laser melting. Materials and Design. 2017;**113**:331-340. DOI: 10.1016/j.matdes.2016.10.037

[61] Wilkes J, Wissenbach K. Rapid manufacturing of ceramic components for medical and technical applications via selective laser melting. Conf Euro-uRapid 2006:A4

[62] Zaragoza-Siqueiros J, Medellín-Castillo HI. Design for rapid prototyping, manufacturing and tooling: Guidelines. In: ASME International Mechanical Engineering Congress and Exposition Volume 2A: Advanced Manufacturing. ASME; 2014. p. V02AT02A013. DOI: 10.1115/IMECE2014-39310

[63] Liu Q, Danlos Y, Song B, Zhang B, Yin S, Liao H. Effect of high-temperature preheating on the selective laser melting of yttria-stabilized zirconia ceramic. Journal of Materials Processing Technology. 2015;**222**:61-74. DOI: 10.1016/J.JMATPROTEC.2015.02.036

[64] Liu Q, Song B, Liao H. Microstructure study on selective laser melting yttria stabilized zirconia ceramic with near IR fiber laser. Rapid Prototyping Journal. 2014;**20**(5):346-354. DOI: 10.1108/RPJ-12-2012-0113

[65] Kruth JP, Froyen L, Van Vaerenbergh J, Mercelis P, Rombouts M, Lauwers B. Selective laser melting of iron-based powder. Journal of Materials Processing Technology. 2004;**149**(1–3):616-622. DOI: 10.1016/j.jmatprotec.2003.11.051

[66] Savchenko NL, Sablina TY, Kul'kov SN. Influence of annealing on the phase composition of vacuum-sintered material ZrO_2-3 (mole)% Y_2O_3. Powder Metallurgy and Metal Ceramics. 1996;**34**(3–4):167-171. DOI: 10.1007/BF00559562

[67] Exner H, Horn M, Streek A, Ullmann F, Hartwig L, Regenfuß P, et al. Laser micro sintering: A new method to generate metal and ceramic parts of high resolution with sub-micrometer powder. Virtual and Physical Prototyping. 2008;**3**(1):3-11. DOI: 10.1080/17452750801907970

[68] Tang Y, Fuh JYH, Loh HT, Wong YS, Lu L. Direct laser sintering of a silica sand. Materials and Design. 2003;**24**(8):623-629. DOI: 10.1016/S0261-3069(03)00126-2

[69] Su X, Yang Y. Research on track overlapping during selective laser melting of powders. Journal of Materials Processing Technology. 2012;**212**(10):2074-2079. DOI: 10.1016/J.JMATPROTEC.2012.05.012

[70] Wang J, Qian F, Cheng X. Preliminary study on heat-pressed glass ceramic material II. Biological safety evaluation of material. Journal of Comprehensive Stomatology. 2001;**3**:173-175. Available from: http://en.cnki.com.cn/Article_en/CJFDTOTAL-KQYZ200103004.htm

[71] Zhang B, Qian F, Duan X, Wu B. Study on some mechanism of leucite microcrystallization to reinforce dental glass ceramics. Zhonghua Kou Qiang Yi Xue Za Zhi. 2002;**37**(4):260-264. Available from: http://www.ncbi.nlm.nih.gov/pubmed/12411171

[72] Schweiger M. Zirconiumdioxid – Hochfeste und bruchzähe Strukturkeramik. Ästhetische Zahnmedizin. 2004;**5**:248-257

[73] Lammert T. Aluminiumoxid/Al_2O_3. In: DKG–Technische Keramische Werkstoffe. Fachverlag Deutscher Wirtschaftsdienst, Köln.; 1992

[74] Burger W. Umwandlungs- und plateletverstärkte Aluminiumoxidmatrixwerkstoffe. (Teil 1). Keramische Zeitschrift. 1997;**49**(12):1067-1070

[75] Frazier WE. Metal additive manufacturing: A review. Journal of Materials Engineering and Performance. 2014;**23**(6):1917-1928. DOI: 10.1007/s11665-014-0958-z

[76] Murr LE, Gaytan SM, Ramirez DA, Martinez E, Hernandez J, Amato KN, et al. Metal fabrication by additive manufacturing using laser and electron beam melting technologies. Journal of Materials Science and Technology. 2012;**28**(1):1-14. DOI: 10.1016/S1005-0302(12)60016-4

[77] Song B, Zhao X, Li S, Han C, Wei Q, Wen S, et al. Differences in microstructure and properties between selective laser melting and traditional manufacturing for fabrication of metal parts: A review. Frontiers of Mechanical Engineering. 2015;**10**(2):111-125. DOI: 10.1007/s11465-015-0341-2